Two-dimensional free surface flow numerical model for vertical slot fishways

JACQUES CHORDA (IAHR Member), *Université de Toulouse, INPT, UPS, IMFT (Institut de Mécanique des Fluides de Toulouse), Allée Camille Soula, F-31400 Toulouse, France; and CNRS, IMFT, F-31400 Toulouse, France.*
Email: chorda@imft.fr (author for correspondence)

MARIE MADELEINE MAUBOURGUET, *Université de Toulouse, INPT, UPS, IMFT (Institut de Mécanique des Fluides de Toulouse), Allée Camille Soula, F-31400 Toulouse, France; and CNRS, IMFT, F-31400 Toulouse, France.*
Email: maubourg@imft.fr

HÉLÈNE ROUX, *Université de Toulouse, INPT, UPS, IMFT (Institut de Mécanique des Fluides de Toulouse), Allée Camille Soula, F-31400 Toulouse, France; and CNRS, IMFT, F-31400 Toulouse, France.*
Email: roux@imft.fr

MICHEL LARINIER, *Université de Toulouse, INPT, UPS, IMFT (Institut de Mécanique des Fluides de Toulouse), Allée Camille Soula, F-31400 Toulouse, France; and CNRS, IMFT, F-31400 Toulouse, France.*
Email: larinier@imft.fr

LAURENT TARRADE, *Laboratoire d'Etudes Aérodynamiques, CNRS, Université de Poitiers, ENSMA, SP2MI, Téléport 2, 89962, Futuroscope Chasseneuil Cedex, France.*

LAURENT DAVID, *Laboratoire d'Etudes Aérodynamiques, CNRS, Université de Poitiers, ENSMA, SP2MI, Téléport 2, 89962, Futuroscope Chasseneuil Cedex, France.*
Email: Laurent.David@univ-poitiers.fr

ABSTRACT
Numerical results of a vertical slot fishway study are presented. The Saint–Venant equations are solved using TELEMAC-2D. Turbulence modelling uses the classical two equations $k-\varepsilon$ closure model. A comparison with velocity measurements performed at the Laboratoire d'Etudes Aérodynamiques of University of Poitiers, France, using particle image velocimetry and acoustic Doppler velocimetry permitted to validate numerical results. Turbulence modelling is required not only to have a fish-friendly flow but, more remarkably, by the fact that taking a constant eddy viscosity model gives incorrect mean flow patterns. Three longitudinal slopes were tested. The validity of the $k-\varepsilon$ closure model is discussed. Special attention was paid to the calculated turbulent kinetic energy and the energy dissipation rate. This last parameter is of great interest because its spatial distribution significantly affects the progress relative to fish passage efficiency.

Keywords: 2D free surface modelling, energy dissipation, finite-element model, turbulence model, vertical slot fishway

1 Introduction

A vertical slot fishway (VSF) consists of a sequence of pools connected by narrow vertical slots (Rajaratnam *et al.* 1986, 1992, Clay 1995). To prevent fish from excessive velocities, the total hydraulic drop is partitioned into limited water falls localized at each slot, the water fall equalling the product of the longitudinal slope times pool length. The main VSF characteristics are quasi-insensitivity of flow to discharge variation, and flow depth varying about linearly with discharge (Wu *et al.* 1999).

To satisfy the European directive requiring the extension of fish passes efficiency to any fish species and particularly to small fish at horizon 2015, a better knowledge of the flow structure is required (Baumgartner and Harris 2007, Heimerl *et al.* 2008). To optimize the internal VSF geometry, Alvarez-

Vazquez *et al.* (2008a,b) formulated and solved an optimal control problem with an original approach. Their cost function reflects the need of rest areas for fish and of a flow velocity suitable for fish swimming capabilities, based upon a mix of maximum velocity and vorticity intensities. However, this understanding should not be limited to mean values but must be extended to velocity fluctuations to locate areas of high turbulence level, to which fish is highly sensitive (Pavlov *et al.* 2000, Odeh *et al.* 2002, Nikora *et al.* 2003, Rodriguez *et al.* 2006).

The nature of VSF free surface flows, induced by dissymmetrical confined jets in successive pools, appears to be highly complex. Nevertheless, despite the strong three-dimensional (3D) local velocity gradient in the slot zone at water fall location, flows in the major part of the pool are quasi two-dimensional (2D) with small vertical velocities relative to the horizontal (Wu *et al.* 1999, Liu *et al.* 2006). The 3D effects increase with the longitudinal slope if eddies, flow separations, vortices, up- and down-wellings are amplified.

Until recently, this flow complexity implied the exclusive use of expensive scale models to control and guarantee flow characteristics in accordance with fish capacities (Liu 2004, Pena *et al.* 2004, Puertas *et al.* 2004, Liu *et al.* 2006, Rodriguez *et al.* 2006). Recent extensive experiments performed at the Laboratoire d'Etudes Aérodynamiques (LEA) using particle image velocimetry (PIV) and acoustic Doppler velocimetry (ADV) tests by Tarrade *et al.* (2008) include a valued database for the flow topology and turbulence properties such as root mean squared velocity fluctuations, vortex length scales, and turbulent kinetic energy k. These strongly influence fish passage (Clay 1995, Nikora *et al.* 2003, Guiny *et al.* 2005, Cheong *et al.* 2006). Currently, fully operational 2D free surface codes are available providing average flow characteristics at each mesh node, including water surface elevation, velocity components, dynamic pressure, local vorticity, k, and energy dissipation rate. Cea *et al.* (2007a) applied a finite volume code solving the depth averaged Saint-Venant equations to model a VSF and compared several 2D turbulence models.

TELEMAC-2D (Hervouet 2000) was used herein, an unsteady 2D free surface hydrodynamics finite-element code, similar to that of Cea *et al.* (2007a). They cited experimental studies by Rajaratnam *et al.* (1986, 1992), Pena *et al.* (2004), and Puertas *et al.* (2004), indicating that the mean velocity field in the pool is quasi-2D, that is, the vertical velocity magnitude being much smaller than the horizontal. The 2D shallow-water modelling used in the TELEMAC-2D code is a priori applicable except for the slot region, where the hydrostatic pressure assumption does not apply.

After a definition of the tested VSF geometry and the description of the main flow characteristics obtained from the experiments, the numerical model, its parameters, and the boundary conditions are described. The validation of TELEMAC-2D results involves a comparison with LEA measurements and the turbulence modelling will be discussed prior to the application of the numerical results to fishway analysis.

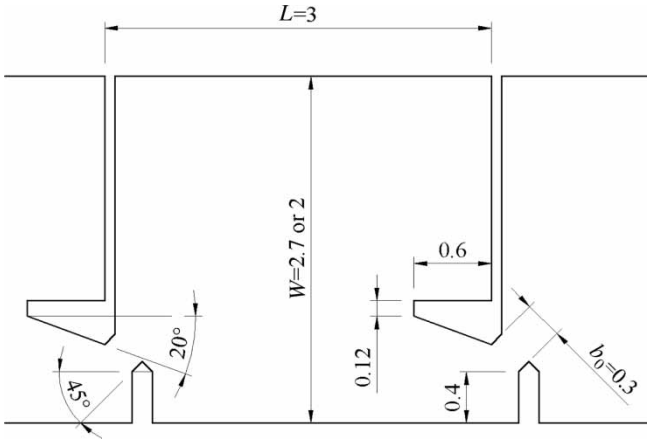

Figure 1 Fish pass geometry, with dimensions expressed in metres.

2 Vertical slot fishway design

The fishpass geometry is shown in Fig. 1. Main dimensions are slot width $b_0 = 0.3$ m, basin length $L = 3$ m, and two tested widths $W = 2$ m or 2.70 m. Length and width proportions are $L/b_0 = 10$ and $W/b_0 = 6.6$ or 9, respectively. These standard values are issued from current VSF designs (Rajaratnam *et al.* 1992, Clay 1995) and used for recent experimental studies (Stuart and Mallen-Cooper 1999, Wu *et al.* 1999, Stuart and Berghuis 2002, Liu 2004, Pena *et al.* 2004, Puertas *et al.* 2004, Liu *et al.* 2006, Rodriguez *et al.* 2006). The baffle design results from numerous laboratory and *in situ* studies (Rajaratnam *et al.* 1992, Clay 1995, Larinier and Marmulla 2003). This internal design promotes fish migration of salmon, shad, and sea trout.

3 Experimental setup

Experimentation was made in LEA using a 1 : 4 scale model (Tarrade 2007), relating to Froude similitude. The VSF model consisted of five pools of internal geometry similar to Fig. 1. The walls and the floor were made of Plexiglas to allow for flow visualization and laser operation (Fig. 2). The tilting channel allowed for slope variations from 5 to 15%. The discharge was measured via an electromagnetic flowmeter to $\pm 0.5\%$. The tailwater was controlled by an adjustable plate weir to reach uniform flow for a given slope, discharge, and width.

A discharge of $Q = 23\ \mathrm{ls}^{-1}$, that is, $0.735\ \mathrm{m}^3\mathrm{s}^{-1}$ at prototype scale, was considered. The tests were taken in the third pool to ensure uniform flow as the gravity is balanced by dissipation. The x- and y-axis correspond to the longitudinal and transversal directions. Velocity measurements were taken using PIV (Lloyd *et al.* 1995, Fujita *et al.* 1998) between two planes located at $z/b_0 = 0.26$ and 2 above the bottom. The acquisition and post-processing PIV system were composed of laser light illuminating the flow section, a camera system, and a synchronization unit. The correlator Flowmap PIV 2000 Processor (Dantec®) allowed to synchronize the laser system and the cameras. A laser Nd-Yag double cavity Spectra-Physics (2×200 mJ) was used to

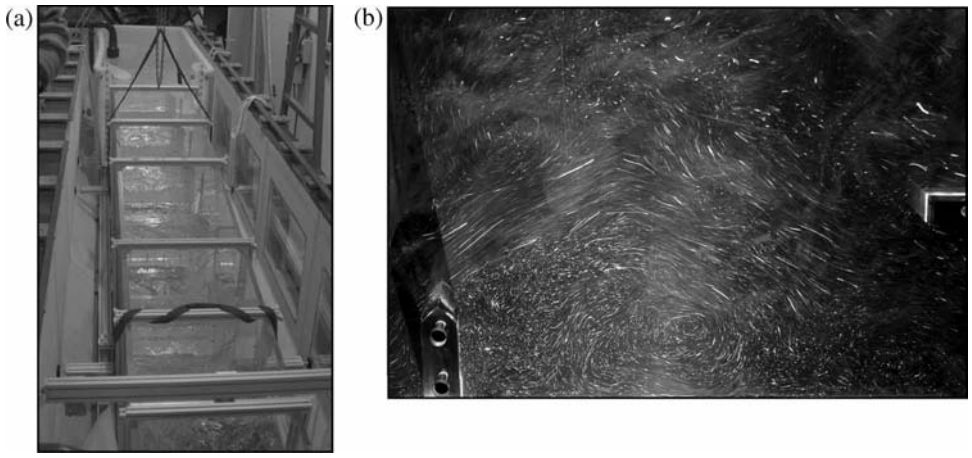

Figure 2 (a) Downstream view of test flume at LEA and (b) pool detail

illuminate a flow section seeded by 11 μm dye particles. The frequency of each cavity is ~10 Hz and the wavelength 532 nm. The beams originating from the two cavities were then conveyed using a telescopic arm towards a system of double lens system to produce a narrow laser sheet of ~1.5 mm thickness. To record successive flow snapshots, two CCD cameras FlowIntense® were used with objectives of 28 mm placed in parallel to visualize the entire pool. Their resolution is 1376 × 1040 pixels^2, coded on 12 bits. The cameras acquire two successive flow images separated between 3000 and 4000 μs, generated between the two laser cavities. The FlowManager software (Dantec®) controls the PIV system, computes cross-correlations between the successive images, and post-processes the calculated data. An initial interrogation area of 64 × 64 pixels^2, a final interrogation area of 32 × 32 pixels^2 with an overlap of 50%, and window deformation were used to compute cross-correlation. For each camera, five bursts of 175 image acquisitions, separated by 200 ms allow to capture 875 instantaneous velocity fields to be averaged. The two mean velocity fields calculated are combined to provide the complete mean velocity field and additional characteristics as streamlines. The accuracy of this PIV technique was relatively low due to the large field recorded (0.75 × 0.65 m^2), the small displacements measured, the presence of background noise, the window size, and post-processing which reduced the amplitudes of velocity gradients.

To complete the PIV measurements and to obtain a full 3D pattern of local velocity components, ADV measurements were performed by Tarrade (2007) along various vertical profiles using a micro ADV Sontek® 3D-probe. This metrology, based upon the analysis of the Doppler shift frequency generated by echoes backscattered by solid particles or micro bubbles, allows to measure 3D-velocity components (Blanckaert and Lemmin 2006). The maximum sampling frequency was 50 Hz and the sample volume extension was 0.09 cm^3. The signal-to-noise is around 25–30 dB with a signal correlation between 70 and 100%. The recording time is 120 s. Due to the presence of parasite echoes because of wall reflection and noise artefacts, several filtering methods are applied to correct values corresponding to low correlated echoes (Nikora *et al.* 1998, Wahl 2000, Goring and Nikora 2002, Cea *et al.* 2007b). The accuracy is not simple to define, but is always linked to the original signal and the correlation between the three receivers. To compare between PIV and ADV measurements, differences between the measurement volume, recording time (frequency and total time), and signal filtering after acquisition explain differences in velocity fluctuations.

4 Flow characteristics in vertical-slot pools

As previously mentioned, VSF pools have been explored on scale models. Most experimental setups had similar slot width ratios of $W/b_0 = 6.7$, $L/b_0 = 10$, and only differed by the shape and orientation of baffles. Tested slopes range typically between $S_o = 5$ and 10%. The highest VSF velocities always occur at communicating slots due to the water fall, a strong jet core and path with significant momentum, jet decay with swirling zones, recirculation zones, and flow reattachment. The difference with a plane jet structure was discussed by Liu *et al.* (2006) with "the growth rate of the jet in the pool being larger than that of a plane turbulent jet". The main flow features are as follows:

- Quasi-invariance of flow characteristics from the third pool because of equilibrium between slope and energy dissipation;
- Quasi-independence of velocity magnitude relative to discharge because its value results from the water fall at each slot;
- Flow depth in pools varying almost linearly with discharge for a given slope (Wu *et al.* 1999).

For $S_o \leq 5\%$, 2D flows were normally recorded, except for the slot zone with the impinging jet. For the same discharge and $S_o = 5$ and 10%, two distinct flow patterns were described by Wu *et al.* (1999) and by stream traces extracted from LEA (Fig. 3).

For $S_o = 5\%$, the jet issuing from the slot crosses the pool axially towards the slot outlet, two large recirculation zones expanding on each side. For $S_o = 10\%$, the upper zone is filled

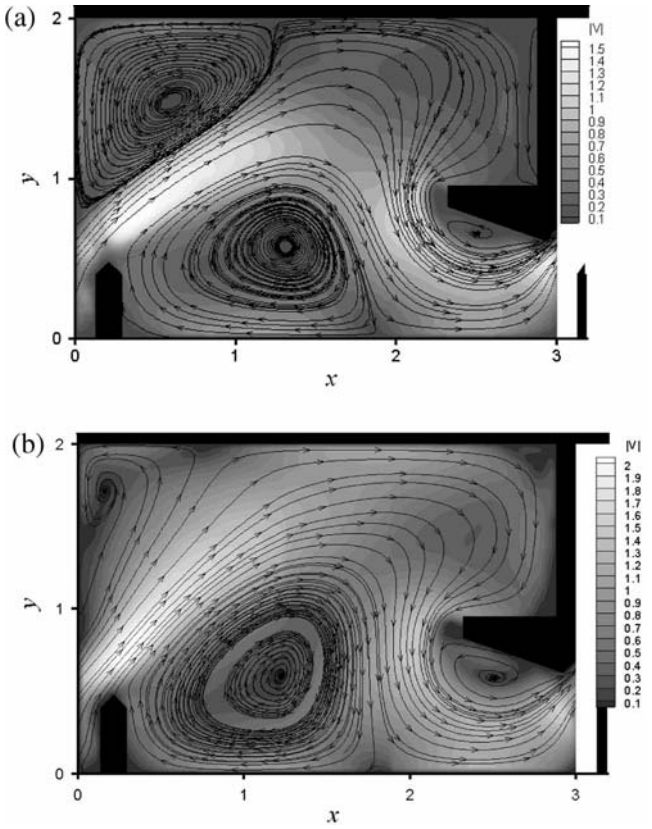

Figure 3 Flow patterns by stream traces from PIV for S_o = (a) 5% and (b) 10% (LEA)

with the left hand jet side and quasi disappears. The jet has enough intensity to impact the downstream wall. A recirculation zone, characterized by small velocities, appeared alongside the short baffles (Liu 2004).

5 The numerical model

5.1 *Model description*

TELEMAC-2D (Hervouet and Petitjean 1999, Hervouet and Jankowski 2000, Hervouet 2003) provides hydrodynamic variables such as flow depth, depth-integrated velocity vector k, eddy viscosity, and energy dissipation rate at each node of an unstructured triangular mesh. Most results presented below relate to a pool width of $W = 2$ m corresponding to $L/W = 1.5$, yet some runs were made for wider pools with $W = 2.7$ m, the pool width modifying the flow topology as shown by LEA tests. For $Q = 0.735$ m^{3}s^{-1}, three values of S_o =5, 10 and 15 % were tested to observe their effect on the flow. The last value stands beyond the commonly accepted upper limit for VSF applications, but is considered interesting for modelling purposes. The numerical modelling was carried out using a configuration consistent with LEA tests, namely an inlet pool, five operating pools, and an outlet pool (Fig. 4). The selected number of pools was shown to be sufficient to obtain fully developed pseudo-uniform flow past the central basins and to eliminate the possible effect of fishway inlet and outlet boundary

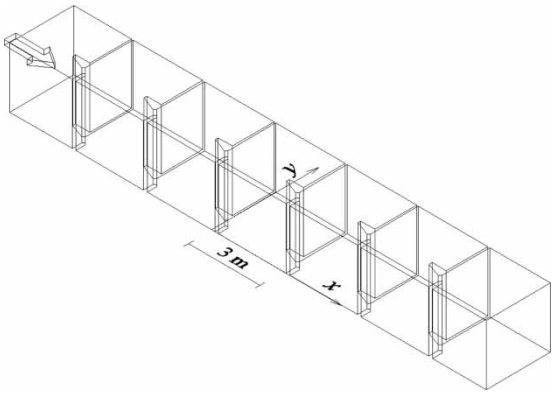

Figure 4 Perspective view of fishway model (five operating pools)

conditions (Heimerl *et al.* 2005). The results and comparisons focus on the third pool, the so called "test pool".

The 2D triangular unstructured grid must not have a too coarse mesh size at slot locations where large flow depths and velocity gradients occur. The slots are hydraulic control sections governing the discharge in relation to the pool water level. Several mesh size distributions were tested, including large density in the slot zones and coarser elsewhere or with a grid size decreasing in the high gradient zones for a grid size of $d \geq 0.03$ m, based on preliminary results. About 10 nodes were located across each slot, in zones corresponding to the highest velocity gradients, near pool entrances, and exits, where the active flow is concentrated. After several tests, the preferred grid size, offering the optimum ratio between quality of results and computing time, was an uniform grid size of $d = 0.03$ m in the "central" pools, paired with a 0.05 m size in the up- and downstream pools (Fig. 5). The total number of nodes used to model 5 fishway pools varies from about 20,000 to 30,000, depending on the pool width.

5.2 *Boundary and initial conditions*

The boundary conditions used were a prescribed constant discharge at the model inlet and a depth-discharge relation at the outlet. Imposed values correspond to the experimental settings. At each time step, the outflow was calculated from the depth values at the outlet nodes using a rating curve relation. The

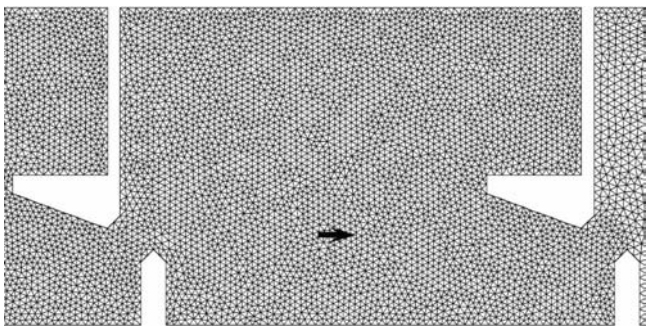

Figure 5 Uniform mesh size 0.03 m in central pools ②③④, and 0.05 m in pools ① and ⑤

outlet velocity distribution was considered uniform. The main benefit of this outlet prescription resides in its continuous self adjustment, which has a significant acceleration effect on the numerical convergence.

Concerning the wall velocity boundary condition, the usual adherence condition leads to use a very dense mesh, particularly near the walls. This method strongly increased the grid density and therefore was abandoned. Following Gorski *et al.* (1985) and Bazilevs *et al.* (2007) who suggest to apply a weak wall condition instead of the classical no slip prescription, a free slip condition $\mathrm{d}V/\mathrm{d}n = 0$ was imposed. For 2D depth-integrated equations, it must be verified that bottom friction is dominant relative to lateral wall friction. This fact results from the flow structure, dominated by recirculation zones with observed velocity intensities along the walls normally weak, except along the slot sides. Herein, this weak condition works fine and flow depths fit with experiments.

5.3 *Computational parameters*

When starting from a rest state of constant water elevation and null velocity, the computational time steps allowing stability and convergence of the calculus finally ranged from 0.005 to 0.05 s, and the overall time of simulation to reach a steady state with a difference between inlet and outlet discharges of less than $10^{-6}\mathrm{m}^3\mathrm{s}^{-1}$ was $\sim$200 s. The friction factor was modelled with Manning's coefficient $n = 0.0105$ $\mathrm{m}^{-1/3}\mathrm{s}$ corresponding to the smooth flume boundaries of Plexiglas. This parameter is not significant because bed friction does not play an important role for this flow type. Cea *et al.* (2007a) found no differences for Manning coefficients ranging between $n = 0$ (no friction) and 0.03 $\mathrm{m}^{-1/3}\mathrm{s}$.

6 Comparison with measurements at LEA

6.1 *Test case*

Knowing that a fish-friendly flow analysis lies upon full scale values (based on fish length for example), it is suitable to express flow depths, velocity magnitudes, and dissipated energy at full scale values. Preliminary runs were made running TELEMAC-2D consecutively at 1 : 4 scale and full scale using the same computational grid. The close agreement of results proved that no scale effects were noticeable. This is due to the fact that the internal pool geometry is important for flow structure. The results for $S_o = 10\%$ and $Q = 0.735$ $\mathrm{m}^3\mathrm{s}^{-1}$ will be presented therefore at full scale.

The measured axial flow depth was 1.12 m and this value was used to fix the discharge level prescribed as downstream boundary condition. The depth-averaged computed values in the reference pool are compared with the upper PIV plane with $z = 2 \times 0.3 = 0.6$ m, located approximately at the mid height of flow.

6.2 *Effect of turbulence model closure*

A customary method for turbulence model closure consists in using a constant value for the eddy viscosity υ_T for the entire computational domain. This practice, frequent in river engineering, gives satisfactory results in the majority of studies (Wilson *et al.* 2002, Vionnet *et al.* 2004). The depth-integrated velocity vector field calculated with TELEMAC-2D was compared with PIV measurement results for $z = 0.60$ m. Figure 6 shows the results obtained using $\upsilon_T = 2 \times 10^{-3}$ $\mathrm{m}^2\mathrm{s}^{-1}$. The slot-issuing jet deviates directly towards the downstream baffle instead of a trajectory towards the left pool bank, as shown by PIV results.

An essential result for flow with swirling zones is that a constant eddy viscosity is quite irrelevant to obtain the mean flow topology. Because of strong hydraulic gradients, particular attention must be paid to turbulence modelling even if only average velocity maps are reproduced.

6.3 *Comparison of results*

Using the k–ε model, the computed depth-integrated mean velocity field matches observations well in the mid-depth plane

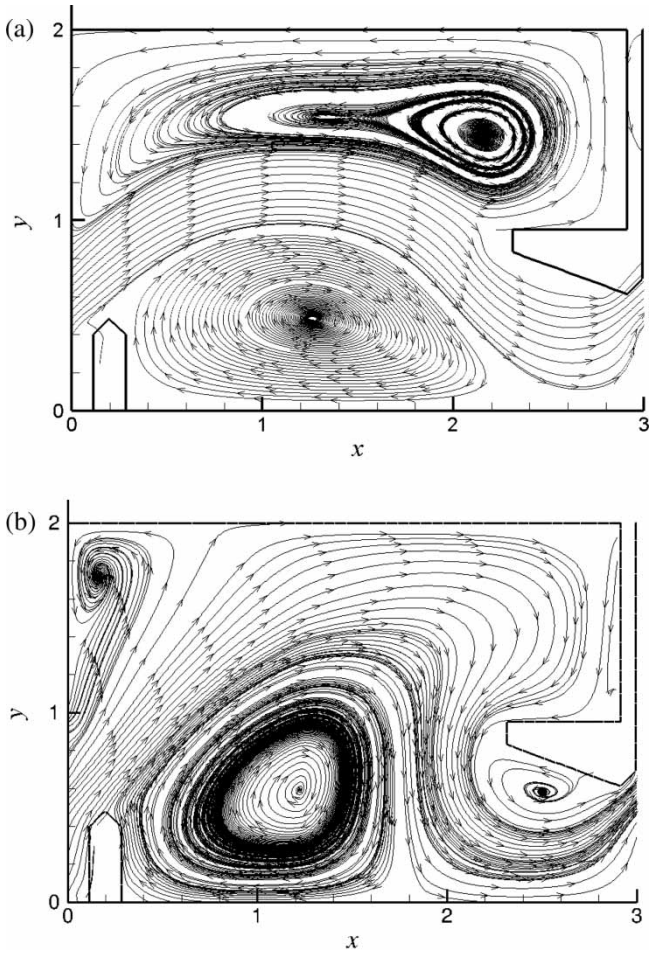

Figure 6 Streamtraces computed for $S_o = 10\%$ and (a) $\upsilon_T = 2 \times 10^{-3}$, (b) PIV

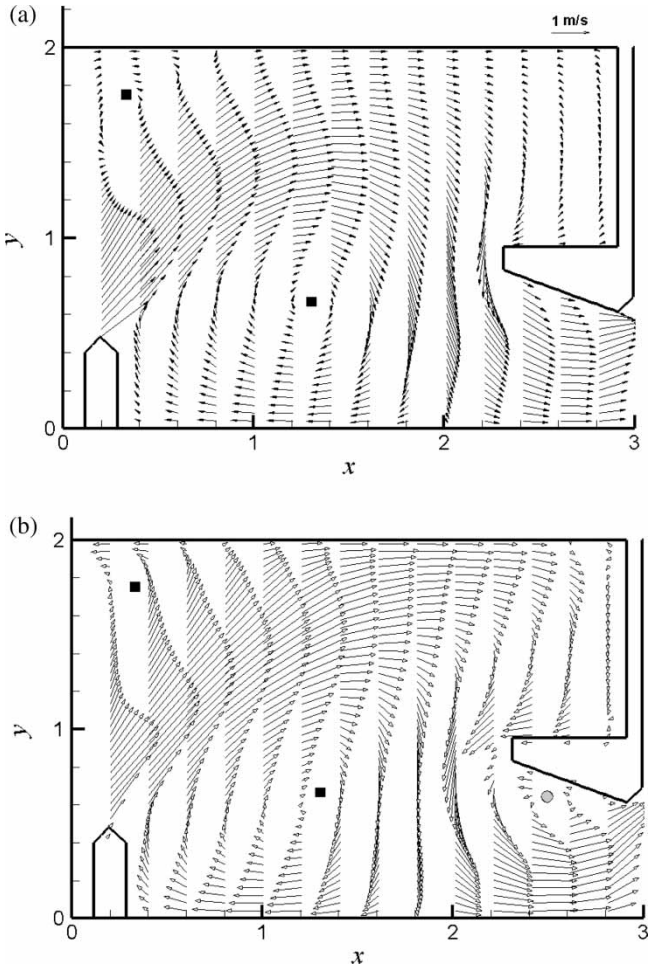

Figure 7 (a) TELEMAC-2D velocity field versus (b) PIV velocity vectors at plane $z = 60$ cm for $W = 2$ m, $S_o = 10\%$, $Q = 0.735$ m^{3}s^{-1} with (filled square) centres of recirculation zones, (filled circle) separation zone

(Fig. 7a). The agreement between the two main recirculating zones is good. The larger is located at about $x = 1.3$ m, $y = 0.65$ m, and corresponds to the right bank baffle wake, the smaller resides at the upper left pool corner at $x \cong 0.3$ m, $y \cong 1.75$ m. The impinging jet trajectory is correct but predicted too low in the upper zone beyond mid-pool length. The computed flow decelerates too much before encountering the downstream baffle wall. As a consequence, the model does not reproduce the separation zone at the deflector wall (Fig. 7b). It seems also that the energy diffusion is too strong in the upper (stagnation) zone due to overestimation of eddy viscosity.

For the pool of width $W = 2.70$ m, velocity maps are compared with measurements in Fig. 8. A good agreement is observed between velocity vectors for $y \leq 2$ m, but a discrepancy corresponding with underestimated values is seen in the upper zone and along the north wall. Both recirculation zones are quasi identical. The upper wall effect on the flow structure is well reproduced by the k–ε model.

Figure 9 shows the computed transverse velocity components (U, V) and k profiles at transverse planes $x = 0.3$ m to 1.5 m for $W = 2$ m. Good agreement for the U component appears

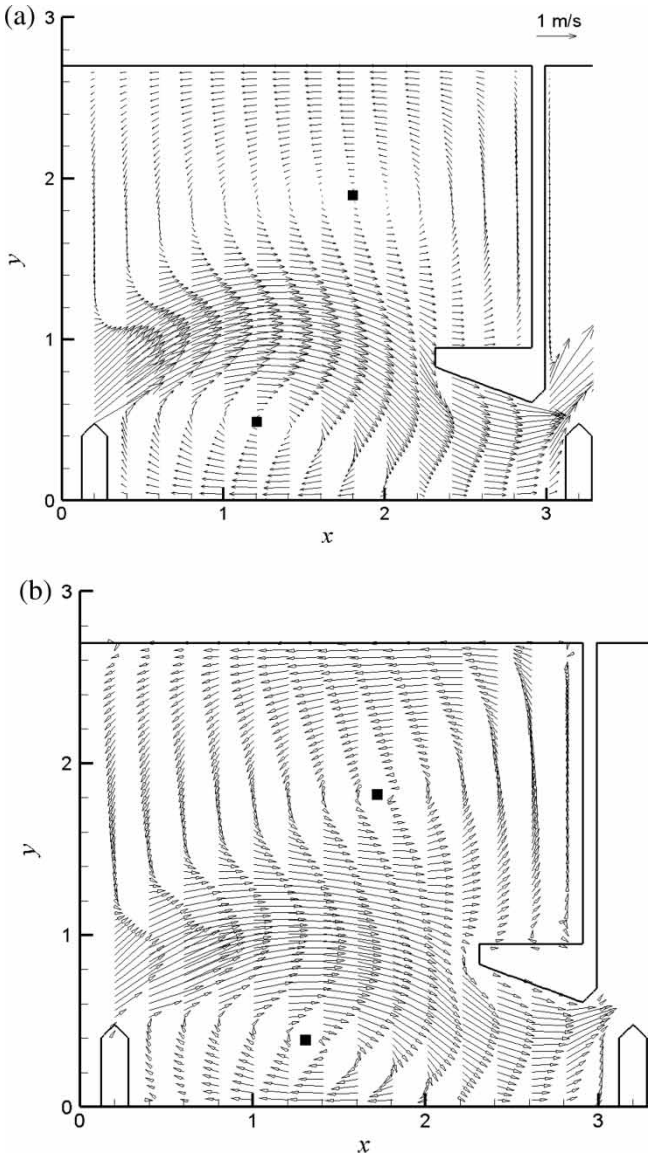

Figure 8 (a) TELEMAC-2D velocity field versus (b) PIV velocity vectors at plane $z = 60$ cm for $w = 2.70$ m, $S_o = 10\%$ and $Q = 0.735$ m^{3}s^{-1} with (filled square) recirculation zones

between the experiment and the TELEMAC results, but differences occur for the V component data issued from ADV and PIV at $x = 1.5$m (Fig. 9e). This bias is mainly due to the poor PIV resolution for small dynamics which is absent for the jet zone (Fig. 9b). To reduce the 3D effect, short time intervals between two laser pulses were used and induced small particle displacements. The accuracy of this technique is then poor and explains these differences. ADV measurements seem to be more reliable.

Significant differences occur relative to the transverse velocity component and to k. In Fig. 9(c)–(f) relating to k, note that despite the 2D assumption, the computed TELEMAC-2D k variable from the k–ε turbulence closure model does correspond to a 3D k variable. The comparison with experiments has to be made after applying a correction to plane 2D PIV, to avoid an underestimation of experimental k values. They were

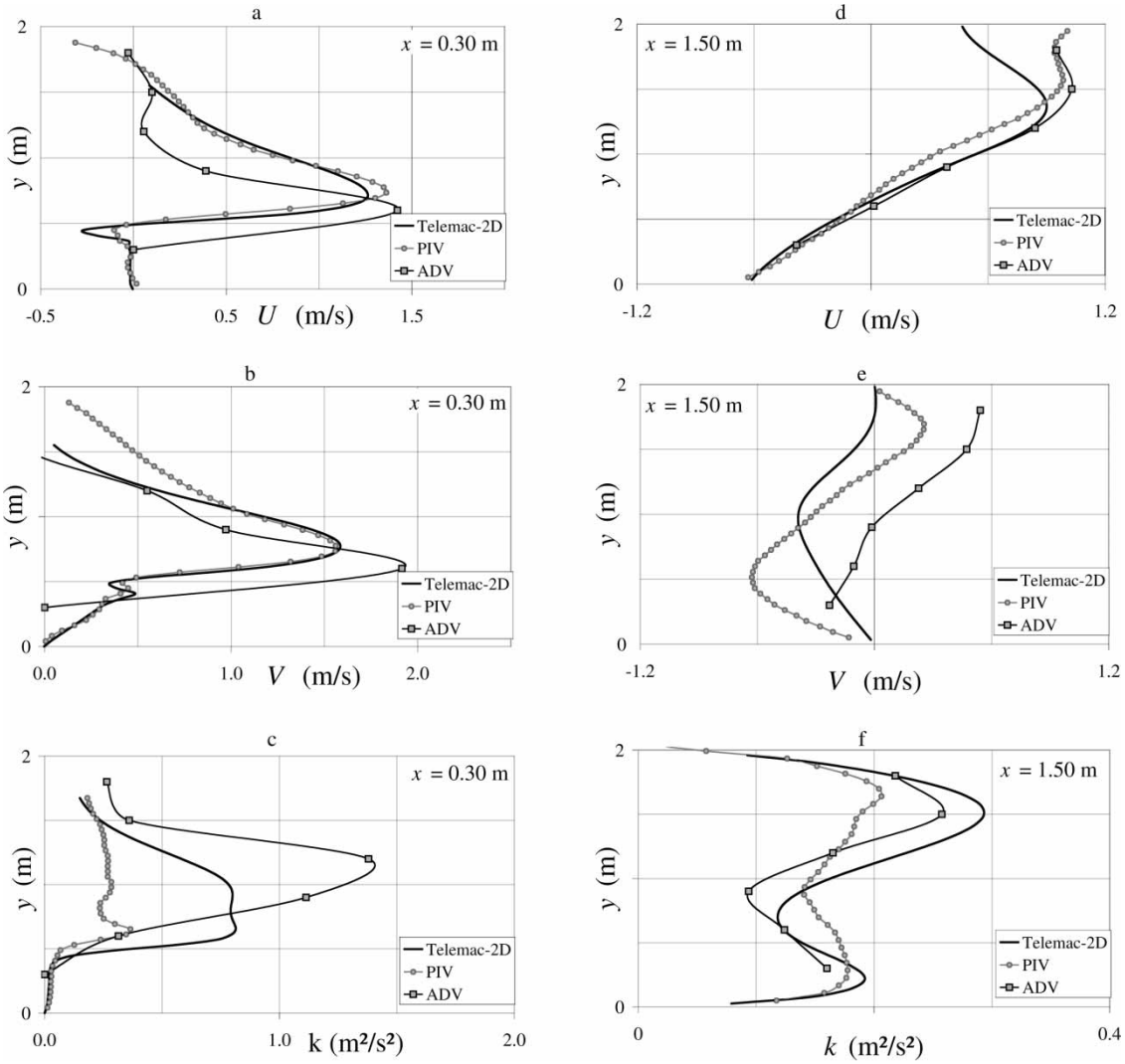

Figure 9 (a), (b) TELEMAC-PIV-ADV velocity components U and V, (c) turbulent kinetic energy at $x = 0.30$ m and (d), (e) U and V, (f) turbulent kinetic energy at $x = 1.50$ m for $w = 2$ m

corrected by the factor 1.33, originating from an isotropic assumption on the fluctuation amplitude, as confirmed by local ADV measurements. Hence, TELEMAC values are compared with ADV and PIV data. Keep in mind that applying the same factor to the entire flow domain is not pertinent and possibly introduces biases at those shown in Fig. 9(c).

Discrepancies between ADV and PIV measurements can be explained by the smoothing effect induced by post-processing and by the low spatial resolution of an interrogation window in PIV. The ADV measurements take into account the three dimensionality of flow with a large effect across the jet (Tarrade 2007). Under-estimation on the one hand (Fig. 9c) and over-estimation on the other (Fig. 9f) explain these differences for the turbulent kinetic energy.

It appears that the longitudinal component U at $x = 1.5$ m obtained with TELEMAC-2D is quite conform to measurements, particularly with ADV, for $y < 1.4$ m (Fig. 9d). The fact that intensities are correct even in the recirculation zone (negative values) is emphasized. However, U velocities are too much damped, as previously mentioned. TELEMAC-2D results are generally located between ADV and PIV data. Further comparison is made relative to k. In the jet zone, the calculated values have a similar evolution to ADV, but the 3D effects are damped (Fig. 9c). At $x = 1.50$ m, the computed values are in agreement with ADV data (Fig. 9f). Concerning the dissipation rate, no comparison is available with LEA measurements.

7 Discussion of $k-\varepsilon$ model

Despite the fact that the $k-\varepsilon$ models permit to deal with complex flows and that reasonably accurate solutions have been obtained for a wide range of industrially relevant flows (Jones *et al.* 2001), its classical default is its poor performance under non-isotropic flow conditions or if strong instabilities develop. Moreover, the stagnation and near-wall regions are not properly solved by most models and often require ad hoc damping functions (Durbin 1996).

Cea *et al.* (2007a) tested three turbulence models for a similar fishway configuration: mixing-length model (MLM), $k-\varepsilon$, and

algebraic Reynolds–Stress model (ARSM) (Rodi 1984). They demonstrated the poor prediction of MLM, but observed that the $k-\varepsilon$ and the ARSM models reproduced fairly well the size of recirculating regions. However, turbulence field values were less accurate than mean velocity if using the Reynolds-averaged Navier Stokes (RANS) models. In the region located downstream the slot inlet, the flow has a strong swirl, with the appearance of separation and reattachment zones within a short distance, which was reported to be far beyond the capabilities of eddy viscosity turbulence models (Cea *et al.* 2007). Their ARSM model gave a better prediction of the turbulence field, the largest differences appearing downstream the slot inlet. The excessively large turbulence level originating from the $k-\varepsilon$ method was reported to be due to the turbulent strain caused by large velocity gradients (up to 20 s^{-1} in their simulations).

The main $k-\varepsilon$ model limitations particularly result from the Boussinesq hypothesis implying that Reynolds stresses are aligned with velocity gradient as expressed by the Reynolds stress expression:

$$\overline{u_i' u_j'} = \frac{2}{3} k \partial_{ij} - 2\upsilon_T S_{ij} \tag{1}$$

The eddy viscosity υ_T and the rate of strain tensor S_{ij} with $i,j =$ indices corresponding to x,y components, $u_i' =$ turbulent velocities fluctuations, $k =$ turbulent kinetic energy and $\delta_{ij} =$ Kronecker symbol are given by

$$\upsilon_T = C_\mu \frac{k^2}{\varepsilon} \quad (C_\mu = 0.09) \tag{2}$$

$$S_{ij} = \frac{1}{2}\left(\frac{\partial U_i}{\partial x_j} + \frac{\partial U_j}{\partial x_i}\right) \tag{3}$$

The anisotropy tensor defined by

$$a_{ij} = \frac{\overline{u_i' u_j'}}{k} - \frac{2}{3}\partial_{ij} \tag{4}$$

can be evaluated using Eq. (1) as

$$a_{ij} = -2\frac{\upsilon_T}{k} S_{ij} \tag{5}$$

The physical limitations are (Wallin and Johansson 2002)

$$-\frac{2}{3} \le a_{ij} < \frac{4}{3} \quad \text{for } i = j \tag{6}$$

$$|a_{ij}| \le 1 \quad \text{for} \quad i \ne j \tag{7}$$

In 2D depth-integrated cases, the three coefficients are:

$$a_{11} = -2\frac{\upsilon_T}{k}\frac{\partial U}{\partial x} \tag{8}$$

$$a_{12} = -2\frac{\upsilon_T}{k}\frac{1}{2}\left(\frac{\partial U}{\partial y} + \frac{\partial V}{\partial x}\right) \tag{9}$$

$$a_{22} = -2\frac{\upsilon_T}{k}\frac{\partial V}{\partial y} = -a_{11} \tag{10}$$

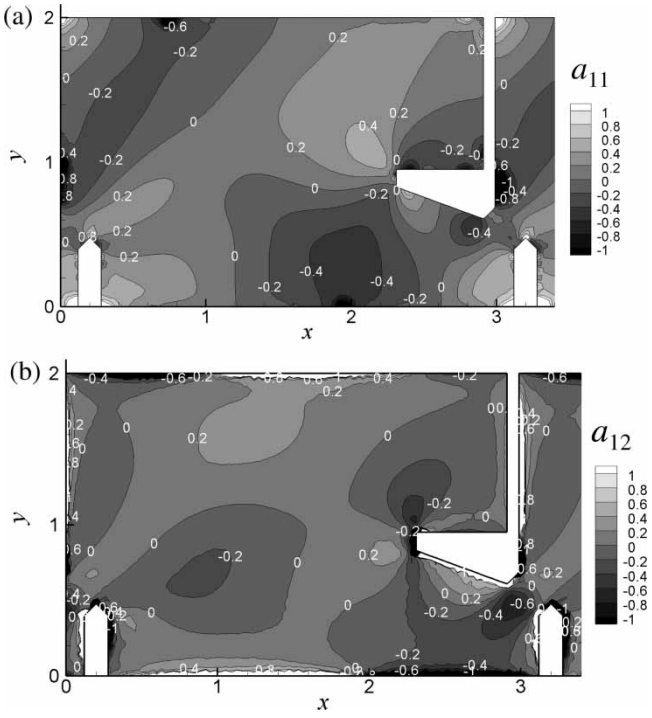

Figure 10 Isotropy tensor coefficients maps from TELEMAC-2D results for $S_o = 15\%$. Results for $S_o = 5$ and 10% are not presented for clarity reasons, but are quasi identical

The coefficients calculated from the results obtained with TELEMAC $k-\varepsilon$ modelling show that the above-mentioned limits are respected except for wall nodes, and that numerical results a priori do not present physically unrealistic features (Fig. 10). This is not a validity proof of the model closure, but a necessary control (Johansson 2002). Moreover, the computed anisotropy tensor a_{ij} has quasi-identical values for $S_o = 5$, 10 and 15%. This characteristic confirms that the 2D horizontal flow structure is quasi invariant with slope. Note that velocity field departures such as observed at the upstream part "nozzle" of the baffle correspond to zones having a strong level of anisotropy.

8 Application to fishway analysis

8.1 *Turbulent kinetic energy*

To observe the effect of longitudinal slope on k, a reference velocity taking the slope into account was defined equal to the maximum velocity given by

$$V_{ref} = \sqrt{2g\Delta H} = \sqrt{2gSL} \tag{11}$$

The turbulent kinetic energy per unit volume is normalized by $0.5V^2_{ref}$ corresponding to the maximum mean flow kinetic energy at the pool inlet. Results are reported in Fig. 11.

Note the good agreement between slopes of 10 and 15%, whereas the dimensionless isolines differ from the case of 5%.

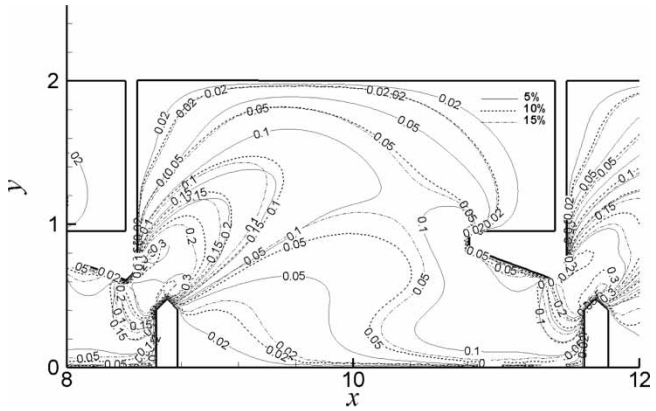

Figure 11 Dimensionless k isoline maps for $S_o = 5$, 10 and 15%

Its relative turbulent level spreads farther in the upper part of the pool corresponding to the jet zone as compared with the larger slopes. This fact may result from a smaller down-welling jet for $S_o = 5\%$ (corresponding to the smallest water drop) and from a longer jet core, therefore. In the lower part, that is, the main recirculation zone, the decay of turbulence is more pronounced than for $S_o = 10$ and 15%. The maximum values exist at the pool inlets, yet restricted to 30% of the maximum kinetic energy.

8.2 *Energy dissipation rate*

As previously mentioned, the spatial distribution of energy dissipation rate is of major importance to evaluate fish adaptability to hydrodynamics. Liu *et al.* (2006) conducted ADV measurements in a VSF and used the Inertial Dissipation Method (IDM) to estimate the dissipation rate ε from the inertial range zone of the power spectrum. The global dissipated power per unit volume P/V_p ($\mathrm{W/m^3}$) with $\rho = 1000$ $\mathrm{kg/m^3}$, $g = 9.81$ $\mathrm{ms^{-2}}$, $\Delta H =$ drop height, $L =$ pool length, and $V_p =$ water volume may be computed from

$$\frac{P}{V_p} = \frac{\varrho g Q \Delta H}{V_p} = \frac{\varrho g Q S L}{V_p} \tag{12}$$

Liu *et al.* (2006) compared the average dissipation rate in a pool issued from the IDM method to global P/V_p values indicating a discrepancy of some 8% for $S_o = 10.52$ and 50% for $S_o = 5.06\%$. The flow geometry, baffle geometry, and the test discharge were too dissimilar from the present to allow for a full comparison. Numerical modelling gives directly the k–ε field values, but limitations inherent to the Saint–Venant 2D depth-integrated equations prevent to accept local dissipation rate values without a global preliminary control. Results obtained for all three slopes and two widths of $W = 2$ m and 2.7 m are compared with the globally dissipated power values in the reference pool. The spatial integral E of TELEMAC-2D ε value is compared with the global P/V_p value. The dimensional values for $Q = 0.735$ $\mathrm{m^3 s^{-1}}$ are summarized in Table 1. Differences are significant but not excessive compared with other works, especially for $W = 2.7$ m, if considering that ε is difficult to estimate from velocity measurements by IDM (Liu *et al.* 2006) and that the present 2D model is based on simplified hypotheses.

As an illustration of results for a fish-friendly flow, Fig. 12 shows isolines of $\rho\varepsilon$ normalized by the maximum value of 200 ($\mathrm{Wm^{-3}}$) commonly adopted for salmon in VSFs (Rodriguez *et al.* 2006), for $Q = 0.735$ $\mathrm{m^3 s^{-1}}$ and all three slopes. For example, a 0.5 isoline value corresponds to a local dissipation rate of $0.5 \times 200 = 100$ $\mathrm{Wm^{-3}}$. The isolines range from 0.05 (10 $\mathrm{Wm^{-3}}$) to 1 (200 $\mathrm{Wm^{-3}}$). Upper values are not significant and correspond to the burst fish capacity speed (Liu 2004) used to pass through the slots. Percentages of the pool area exposed to a local dissipation less than a given fish-compatible level are reported in Table 2 for the three slopes.

Observe that for $S_o = 15\%$ the decreasing magnitude of the fish-friendly area is more important than for smaller slopes. This point confirms that this slope is too steep for fishway application.

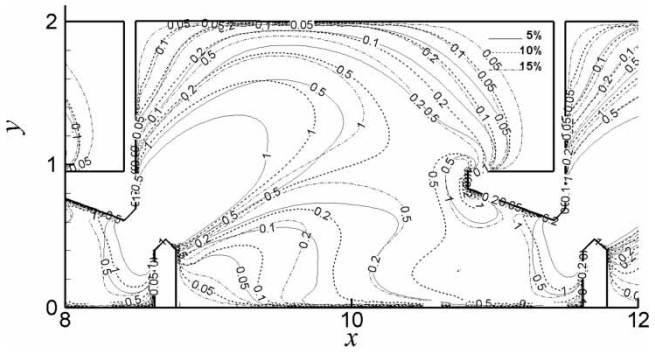

Figure 12 Dissipation rate normalized by P_{ref} [$\mathrm{Wm^{-3}}$] for $S_o = 5$, 10 and 15%

Table 1 Comparison of global P/V with calculated E for $S_o = 5$, 10, 15% and $W = 2$ m, 2.7 m

W (m)	S_o (%)	ΔH (m)	H (m)	P/V_p ($\mathrm{Wm^{-3}}$)	E ($\mathrm{Wm^{-3}}$)	%
2	5	0.15	1.56	116	90	−23
2	10	0.30	1.20	301	220	−27
2	15	0.45	1.10	492	340	−31
2.7	5	0.15	1.6	84	70	−17
2.7	10	0.30	1.25	212	173	−18
2.7	15	0.45	1.13	355	299	−16

Table 2 Area percentages corresponding to local dissipation inferior to a fixed level

S_o (%)	$E < 200$ (Wm^{-3})	$E < 150$ (Wm^{-3})	$E < 100$ (Wm^{-3})
5	91%	88%	82%
10	82%	77%	62%
15	71%	60%	50%

9 Conclusions

A 2D depth-averaged model that is able to perform free surface flow modelling such as TELEMAC-2D appears to be fitted to reproduce correctly the dominant mean velocity and turbulence level fields for mainly 2D flow patterns encountered in a VSF. Tests revealed that a second-order k–ε turbulence closure model is necessary for such flows to reproduce at least the mean velocity flow pattern. Concerning turbulent flow characteristics such as the dissipation rate, which is a major criterion relating to fish adaptation, the k–ε turbulence closure model overestimates turbulence intensity mainly in the slot dependence zone where intense velocity gradients are encountered and correspond to locations where the fish travels upstream through the water fall at burst speed, which is only sustainable for short periods. Nevertheless, the simulated results in the pool have the same order of magnitude as these measured, the values of which lack accuracy due to the strong spatial flow variability. Eddy viscosity turbulence modelling limitations appear, however, in the jet and stagnation zones.

Although the local dissipation rate is a variable, the value of which remains difficult to obtain both from measurement and calculus, this work established limitations but also methods to apply in practice. It demonstrates that a 2D industrial free surface code such as TELEMAC-2D enables to obtain correct flow characteristics in a VSF at low computational cost. This capability allows performing extensive tests on various configurations to minimize experimental tests on scale models, which remain necessary to optimize VSFs and expand their fish-friendly aptitude to small species. Optimizing the design of these fish passes would satisfy the 2015 European directive extending their relevance to small size fish passage.

Notation

b_0 = width of slot (m)
d = grid size (m)
H = water height (m)
k = local turbulent kinetic energy (m^{2}s^{-2})
L = pool length (m)
n = Manning's roughness coefficient (m$^{-1/3}$s)
P = global energy dissipation (Wm^{-3})
Q = discharge (m^{3}s^{-1})
S_{ij} = rate of strain tensor (s^{-1})
S_o = longitudinal slope (–)
U = mean streamwise velocity component (ms^{-1})
u_i' = fluctuating velocity component (ms^{-1})
V = mean transverse velocity component (ms^{-1})
V_p = pool water volume (m^3)
V_{ref} = reference water fall velocity (ms^{-1})
W = pool width (m)
x = streamwise coordinate (m)
y = transverse coordinate (m)
z = vertical coordinate (m)
ΔH = water fall between two consecutive pools (m)
δ_{ij} = Kronecker symbol (–)
ε = local energy dissipation rate (m^{2}s^{-3})
λ = model scale (–)
υ_T = eddy viscosity (m^{2}s^{-1})

References

Alvarez-Vazquez, L.J., Martinez, A., Vazquez-Mendez, M.E., Vilar, M.A. (2008a). An optimal shape problem related to the realistic design of river fishways. *Ecol. Eng.* 32(4), 293–300.

Alvarez-Vazquez, L.J., Martinez, A., Vazquez-Mendez, M.E., Vilar, M.A. (2008b). Vertical slot fishways: Mathematical modeling and optimal management. *Proc. J. Comput. Appl. Math.* 218(2), 395–402.

Baumgartner, L.J., Harris, J.H. (2007). Passage of non-salmonid fish through a Deelder lock on a lowland river. *River Res. Appl.* 23(10), 1058–1069.

Bazilevs, Y., Michler, C., Calo, V.M., Hughes, T.J.R. (2007). Weak Dirichlet boundary conditions for wall-bounded turbulent flows. *Comput. Methods Appl. Mech. Eng.* 196(49–52), 4853–4862.

Blanckaert, K., Lemmin, U. (2006). Means of noise reduction in acoustic turbulence measurements. *J. Hydraulic Res.* 44(1), 3–17.

Cea, L., Pena, L., Puertas, J., Vazquez-Cendon, M.E., Pena, E. (2007a). Application of several depth-averaged turbulence models to simulate flow in vertical slot fishways. *J. Hydraulic Eng.* 133(2), 160–172.

Cea, L., Puertas, J., Pena, L. (2007b). Velocity measurements on highly turbulent free surface flow using ADV. *Exp. Fluids*. 42(3), 333–348.

Cheong, T.S., Kavvas, M.L., Anderson, E.K. (2006). Evaluation of adult white sturgeon swimming capabilities and applications to fishway design. *Environ. Biol Fish* 77(2), 197–208.

Clay, C.H. (1995). *Design of fishways and other fish facilities*. CRC Press, London.

Durbin, P.A. (1996). On the k-3 stagnation point anomaly. *Int. J. Heat Fluid Flow.* 17(1), 89–90.

Fujita, I., Muste, M., Kruger, A. (1998). Large-scale particle image velocimetry for flow analysis in hydraulic engineering applications. *J. Hydraulic Res.* 36(3), 397–414.

Goring, D.G., Nikora, V.I. (2002). Despiking acoustic Doppler velocimeter data. *J. Hydraulic Eng.* 128(1), 117–126.

Gorski, J.J., Govindan, T.R., Lakshminarayana, B. (1985). Computation of three-dimensional turbulent shear flows in corners. *AIAA J.* 23(5), 685–692.

Guiny, E., Ervine, D.A., Armstrong, J.D. (2005). Hydraulic and biological aspects of fish passes for Atlantic salmon. *J. Hydraulic Eng.* 131(7), 542–553.

Heimerl, S., Hagmeyer, M., Echteler, C. (2008). Numerical flow simulation of pool-type fishways: new ways with well-known tools. *Hydrobiologia* 609, 189–196.

Heimerl, S., Hagmayer, M., Kohler, B. (2005). En route with water particules in fishways – how to explain flow structure in a pool-type fishway. Proc. *Hydro2005*, Villach, Austria, 1–15.

Hervouet, J.M. (2000). TELEMAC modelling system: An overview. *Hydrol. Process.* 14(13), 2209–2210.

Hervouet, J.M. (2003). *Hydrodynamique des écoulements à surface libre : Modélisation numérique avec la méthode des éléments finis*. Presses de l'École Nationale des Ponts et Chaussées, Paris [in French], .

Hervouet, J.M., Jankowski, J. (2000). *Comparing numerical simulations of free surface flows using non-hydrostatic Navier–Stokes and Boussinesq equations*. EDF, Paris.

Hervouet, J.M., Petitjean, A. (1999). Malpasset dam-break revisited with two dimensional computation. *J. Hydraulic Res.* 37(6), 777–788.

Johansson, A. (2002). Engineering turbulence models and their development, with emphasis on explicit algebraic Reynolds stress models. *Proc. Conf. Theor. Turbul. Udine*. 253–300.

Jones, R.M., Harvey III, A.D., Acharya, S. (2001). Two-equation turbulence modeling for impeller stirred tanks. *J. Fluids Eng.* 123(3), 640–648.

Larinier, M., Marmulla, G. (2003). Fish passes: Types, principles and geographical distribution – An overview. Proc. 2nd Intl. Symp. *Management of Large Rivers for Fisheries: Sustaining Livelihoods and Biodiversity in the New Millennium*, Phnom Penh, Kingdom of Cambodia, 183–206.

Liu, M. (2004). Turbulence structure in hydraulic jumps and vertical slot fishways, Ph.D. thesis. University of Alberta, Edmonton, CA.

Liu, M., Rajaratnam, N., Zhu, D.Z. (2006). Mean flow and turbulence structure in vertical slot fishways. *J. Hydraulic Eng.* 132(8), 765–777.

Lloyd, P.M., Stansby, P.K., Ball, D.J. (1995). Unsteady surface-velocity field measurement using particle tracking velocimetry. *J. Hydraulic Res.* 33(4), 519–534.

Nikora, V.I., Aberle, J., Biggs, B.J.F., Jowett, I.G., Sykes, J.R.E. (2003). Effects of fish size, time-to-fatigue and turbulence on swimming performance: A case study of Galaxias maculatus. *J. Fish Biol.* 63(6), 1365–1382.

Nikora, V.I., Goring, D.G., Biggs, B.J.F. (1998). Silverstream eco-hydraulics flume: Hydraulic design and tests. *New Zealand J. Marine Freshw. Res.* 32(4), 607–620.

Odeh, M., Noreika, J.F., Haro, A., Maynard, A., Castro-Santos, T., Cada, G.F. (2002). Evaluation of the effects of turbulence on the behavior of migratory fish, *Report* 2000-057-00 to Bonneville Power Administration. Portland, OR.

Pavlov, D.S., Lupandin, A.I., Skorobogatov, M.A. (2000). The effects of turbulence on the behavior and distribution of fish. *J. Ichthyol.* 40(2), S232–S261.

Pena, L., Cea, L., Puertas, J. (2004). Turbulent flow: An experimental analysis in vertical slot fishways. Proc. 5th Intl. Conf. *Ecohydraulics*, Madrid, 881–888.

Puertas, J., Pena, L., Teijeiro, T. (2004). Experimental approach to the hydraulics of vertical slot fishways. *J. Hydraulic Eng.* 130(1), 10–23.

Rajaratnam, N., Katopodis, C., Solanki, S. (1992). New designs for vertical slot fishways. *Canada. J. Civil Eng.* 19(3), 402–414.

Rajaratnam, N., Van der Vinne, G., Katopodis, C. (1986). Hydraulics of vertical slot fishways. *J. Hydraulic Eng.* 112(10), 909–927.

Rodi, W. (1984). *Turbulence models and their applications in hydraulics*. IAHR, Delft.

Rodriguez, T.T., Agudo, J.P., Mosquera, L.P., Gonzalez, E.P. (2006). Evaluating vertical-slot fishway designs in terms of fish swimming capabilities. *Ecol. Eng.* 27(1), 37–48.

Stuart, I.G., Berghuis, A.P. (2002). Upstream passage of fish through a vertical-slot fishway in an Australian subtropical river. *Fisheries Manage. Ecol.* 9(2), 111–122.

Stuart, I.G., Mallen-Cooper, M. (1999). An assessment of the effectiveness of a vertical-slot fishway for non-salmonid fish at a tidal barrier on a large tropical/subtropical river. *Regul. Rivers Res. Manage.* 15(6), 575–590.

Tarrade, L. (2007). Etude des écoulements turbulents dans les passes à poissons à fentes verticales : adaptation aux petites espèces. *Thèse de doctorat*. Université de Poitiers, Faculté des sciences fondamentales et appliquées, Poitiers, [in French].

Tarrade, L., Texier, A., David, L., Larinier, M. (2008). Topologies and measurements of turbulent flow in vertical slot fishways. *Hydrobiol.* 609(1), 177–188.

Vionnet, C.A., Tassi, P.A., Vide, J.P.M. (2004). Estimates of flow resistance and eddy viscosity coefficients for 2D modelling on vegetated floodplains. *Hydrol. Process.* 18(15), 2907–2926.

Wahl, T.L. (2000). Analyzing ADV data using WinADV. Proc. Joint Conf. *Water Resources Engineering and Water Resources Planning & Management*, Minneapolis, 10pp. ASCE, Reston VA.

Wallin, S., Johansson, A.V. (2002). Modelling streamline curvature effects in explicit algebraic Reynolds stress turbulence models. *Int. J. Heat Fluid Flow.* 23(5), 721–730.

Wilson, C.A.M.E., Bates, P.D., Hervouet, J.M. (2002). Comparison of turbulence models for stage-discharge rating curve prediction in reach-scale compound channel flows using two-dimensional finite element methods. *J. Hydrol.* 257(1), 42–58.

Wu, S., Rajaratnam, N., Katopodis, C. (1999). Structure of flow in vertical slot fishway. *J. Hydraulic Eng.* 125(4), 351–360.